DOI: 10.1002/joc.6637

## RESEARCH ARTICLE



## Anchoring of atmospheric teleconnection patterns by Arctic Sea ice loss and its link to winter cold anomalies in East Asia

Muyuan Li<sup>1,2</sup> | Dehai Luo<sup>1,2</sup> | Ian Simmonds<sup>3</sup> | Aiguo Dai<sup>4</sup> | Linhao Zhong<sup>1</sup> | Yao Yao<sup>1</sup>

<sup>1</sup>CAS Key Laboratory of Regional Climate-Environment for Temperate East Asia, Institute of Atmospheric Physics, Chinese Academy of Sciences, Beijing, China

<sup>2</sup>College of earth and planetary sciences, University of Chinese Academy of Sciences, Beijing, China

<sup>3</sup>School of Earth Sciences, The University of Melbourne, Victoria, Australia

<sup>4</sup>Department of Atmospheric and Environmental Sciences, University at Albany, SUNY, Albany, New York

## Correspondence

Dehai Luo, Key Laboratory of Regional Climate-Environment for Temperate East Asia, Institute of Atmospheric Physics, Chinese Academy of Sciences, P. O. Box 9804, West Beichen Rd., Beijing, 100029, China.

Email: ldh@mail.iap.ac.cn

## **Funding information**

Australian Research Council Grant, Grant/Award Number: DP16010997; Chinese Academy of Science Strategic Priority Research Program, Grant/Award Number: XDA 19070403; National Key Research and Development Program of China, Grant/Award Number: 2016YFA0601802; U.S. National Oceanic and Atmospheric Administration, Grant/ Award Number: Award NA18OAR4310425; U.S. National Science Foundation, Grant/Award Number: OISE-1743738

#### **Abstract**

In this paper, the physical processes underlying recent winter cold anomalies over East Asia (EA) are examined via statistical analysis. It is found that the EA cold anomaly depends on the warming in the North Atlantic, sea ice loss in the Barents-Kara Sea (BKS), and atmospheric teleconnection patterns. Specifically, the sea ice loss in the BKS can anchor teleconnection patterns originating from different North Atlantic sea surface temperature (SST) patterns. Different patterns of North Atlantic warming can affect the position of the cold anomaly region through altering the atmospheric circulations. In addition, whether the relevant teleconnection pattern leads to enhanced cold anomaly over EA crucially depends on the sea ice loss in the BKS, because it can anchor the blocking anticyclone embedded in the teleconnection pattern over the Ural region and make it more persistent and quasi-stationary. Furthermore, it is found that the role of SST modes in the EA cold anomaly depends on their time scales. Although the strong basin-scale warming (north-south SST tripolar mode) in the North Atlantic mid- to high-latitudes plays a major role in decadal (interannual) cold anomaly over EA, it appears that the Atlantic east-west SST dipole structure dominates winter temperature variations over EA in recent decades on both the interannual and decadal time scales.

#### KEYWORDS

Arctic climate change, Arctic Sea ice loss, atmospheric teleconnection pattern, East Asia climate, North Atlantic SST mode, winter cold anomaly

## 1 | INTRODUCTION

The Arctic region has experienced amplified warming and a rapid loss of sea ice in winter since the 1990s (Screen and Simmonds. 2010; Walsh, 2014; Simmonds, 2015), whereas East Asia (EA) has shown a large cooling trend during the winter months (Cohen et al., 2014; Mori et al., 2014; Kug et al., 2015; Chen et al., 2018a). However, whether there is a direct connection between these two occurrences is far from clear. Various climate model investigations undertaken with prescribed reductions of Arctic ice present ambiguous results, and many argue that remote responses are barely detectable above natural variability (Screen et al., 2013, 2014). Numerous analyses are now pointing to the role of mediating factors, which may influence whether a significant remote response is induced. For example, many studies have concluded that the winter cold anomaly over EA is associated with the reduced Arctic sea ice (Petoukhov and Semenov, 2010; Outten and Esau, 2012; Cohen et al., 2014; Mori et al., 2014; Kug et al., 2015) through the increased persistence of blocking in the Ural mountains (UB, Luo et al., 2016), while some modelling studies (e.g., McCusker et al., 2016; Dai and Song, 2020) have shown that decreasing Arctic sea ice under increasing CO2 would not cause cooling over EA. Therefore, it seems that the annual to decadal relationship between Arctic sea ice and EA winter temperature anomalies, which result primarily from internal variability, may differ from that of CO<sub>2</sub>-forced long-term changes. Such a potential difference has not been fully appreciated in the literature, and it may have contributed to the ongoing debate regarding Arctic role in causing the recent EA cooling (Cohen et al., 2018).

Some studies have attributed the recent cooling over Eurasia and the loss of Arctic sea ice in winter to recent anomalies in the North Atlantic sea surface temperature (SST), because the teleconnection wave trains that influence the Eurasian climate are mainly a result of forcing of the SST in the North Atlantic (Li, 2004; Sato et al., 2014; Simmonds and Govekar, 2014). The North Atlantic SSTs show significant variations on interannual, decadal and multidecadal timescales (Deser and Blackmon, 1993; Gulev et al., 2013) and have been recognized as a modulator of the global-mean air temperature and air temperatures in the northern hemisphere (Dai et al., 2015; Steinman et al., 2015). However, few studies have focused on the effects of some typical SST warming patterns on the cold anomalies in the EA on different time scales. In addition, the role of the Barents-Kara Sea (BKS) sea ice loss in the persistence of the incoming teleconnection wave trains resulting from the North Atlantic is still unclear. Therefore, this study investigates the role-played by key SST patterns in the North Atlantic on interannual and decadal timescales and quantitatively measured the movement of anticyclonic blockings influenced by the loss of sea ice in the BKS. The SST patterns are obtained by the empirical orthogonal function (EOF) analysis.

## 2 | DATA AND METHODS

## 2.1 | Data

We used monthly mean SST and sea ice concentration (SIC) data on  $1^{\circ} \times 1^{\circ}$  grids for the winter months (December-January-February) during the time period December 1958 to February 2017 from the Hadley Centre Global Sea Ice and Sea Surface Temperature (HadISST) data set (Rayner et al., 2003). Monthly data for the winter surface air temperature (SAT) were obtained from the GISS Surface Temperature Analysis with a resolution of  $2^{\circ} \times 2^{\circ}$  (Hansen et al., 2010). Monthly and daily data for the winter 500-hPa geopotential height (Z500) were taken from the National Centers for Environmental Prediction-National Center for Atmospheric Research reanalysis data set from December 1958 to February 2017 with a resolution of  $2.5^{\circ} \times 2.5^{\circ}$  (Kalnay et al., 1996). The time period December 1958 to February 2017 was chosen because of increased in situ observations and drifting stations in the polar regions after the International Geophysical Year (Raspopov et al., 2007). The linear trend of each variable at each grid point during 1958-2017 is removed. In addition, the effective degrees of freedom are considered when calculating the statistical significance for correlation coefficients.

## 2.2 | Leading patterns in SST anomalies

EOF analysis was used to represent the key modes of variability of the winter monthly North Atlantic (20°-70°N, 100°W-25°E) SST anomalies. From the EOF analysis we extract the first four modes. Together they explain 53.7% of the variance, and each has a clear physical interpretation (see Section 3). The temporal spectra of their PCs were obtained using the fast Fourier transform function in the NCAR Command Language (http://www.ncl.ucar.edu/Document/Functions/list\_alpha.shtml#S).

## 2.3 | Identification of blocking events

The one-dimensional blocking index proposed by Tibaldi and Molteni (1990) was used to identify blocking events

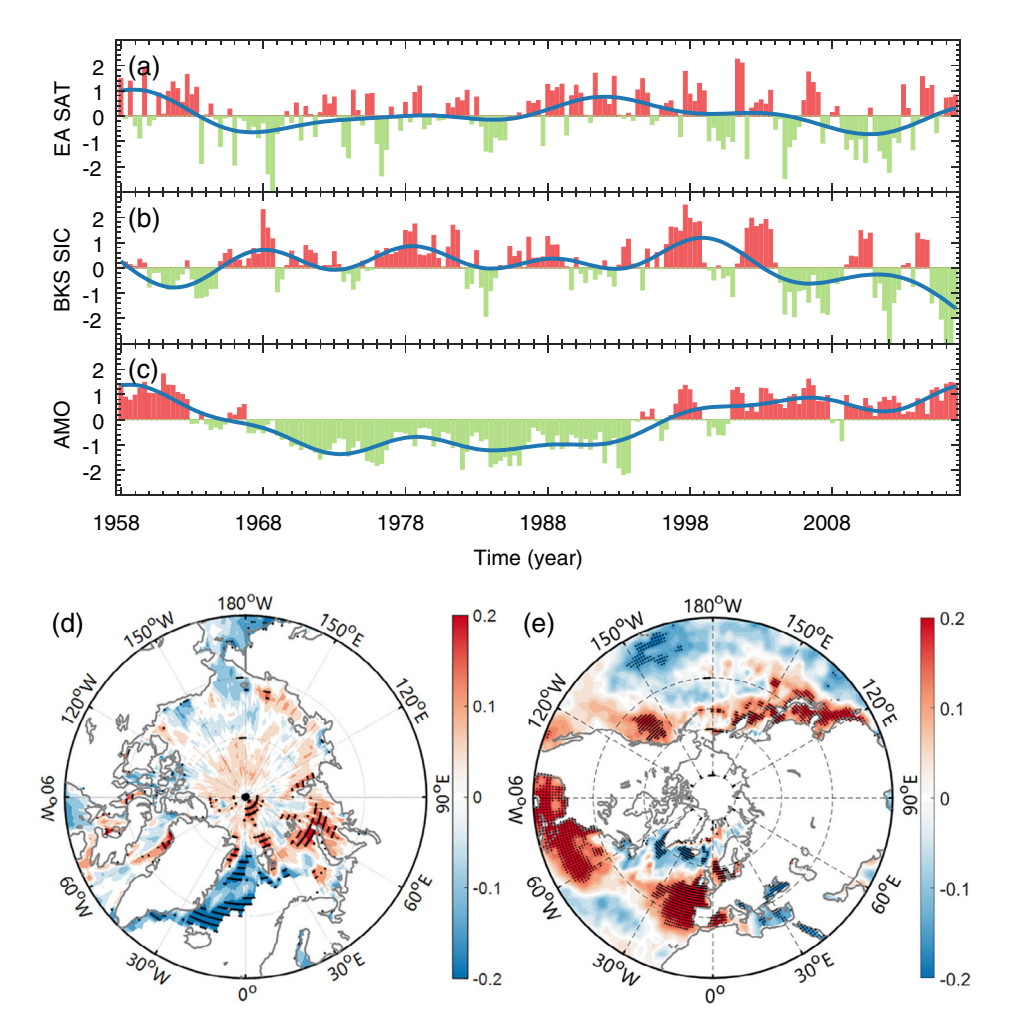
in the Ural region (30-90°E). The index is defined in terms of the Z500 gradients, namely  $GHGN = \frac{Z500(\varphi_N) - Z500(\varphi_0)}{\varphi_0 - \varphi_0}$  and  $GHGS = \frac{Z500(\varphi_0)}{\varphi_0 - Z500(\varphi_S)}$ three given latitudes:  $\varphi_N = 80^{\circ} \text{N} + \Delta$ ,  $\varphi_S = 40^{\circ} \text{N} + \Delta$  and  $\varphi_0 = 60^{\circ}\text{N} + \Delta$  at each longitude ( $\lambda$ ), where  $\Delta = -4^{\circ}$ ,  $0^{\circ}$  or 4°. A blocking event is defined to occur in a given region if the two criteria GHGS > 0 and GHGN < -10gpm·deg<sup>-1</sup> latitude on 12 contiguous longitudes are satisfied for at least five consecutive days. The duration of a blocking event is defined by the number of consecutive days with domain-averaged Z500 anomalies over the region (40-80°E, 50-80°N) exceeding 80 gpm and lag 0 denotes the day with the largest domain-averaged Z500 anomaly.

## 3 | RESULTS

Correlation analysis shows that the SAT in EA has a significant positive (negative) correlation with the SIC anomaly in the BKS (Greenland Sea) (Figure 1d), which suggests that the cold anomalies in EA is probably related

to the decrease in the SIC in the BKS (Petoukhov and Semenov, 2010; Outten and Esau, 2012; Cohen et al., 2014; Mori et al., 2014; Kug et al., 2015) and increase in the SIC in the Greenland Sea (Luo et al., 2017a). Chen and Luo (2017) found that the sea ice loss in the Greenland Sea tends to cause enhanced westward movement and increased persistence of Greenland blocking to influence the North American continent. In contrast, sea ice increase in the Greenland Sea tends to avail cold anomalies over Eurasia. Herein, we further focus on examining their possible connections with the SIC loss in the BKS. We note that the correlation coefficient between the time series for the SAT in EA (Figure 1a) and the BKS SIC (Figure 1b) is 0.14, which is not significant at the 90% significance level. Thus, although there may be a relationship between the cold anomaly in EA and the decrease in the BKS SIC, the nature of it is unclear. Similarly, the monthly mean Multidecadal Oscillation (AMO) (Figure 1c) was not significantly correlated with the SAT in EA, indicating that the cold anomaly in EA is not directly connected to the whole-basin warming related to the AMO, although the AMO has a delayed effect on cold

FIGURE 1 Time series of linearly detrended normalized domain-averaged monthly mean winter (December, January and February). (a) SAT anomalies over East Asia (EA, 80-140°E, 30-60°N), (b) SIC anomalies over the Barents-Kara Sea (BKS, 30-80°E, 65-80°N) and (c) the AMO index defined by a domain-average of SST anomalies over the region  $(80^{\circ}\text{W}-0^{\circ}, 10-70^{\circ}\text{N})$ during the time period 1958-2016. The blue solid lines represent the time variation for periods  $\geq$ 10 years. (d, e) Correlation maps of the linearly detrended (d) SIC and (e) SST anomalies with the normalized EA STA time series during the time period 1958-2016. Stippling represents the area above the 95% confidence level for a two-sided Student's t test [Colour figure can be viewed at wileyonlinelibrary.com]



EOF2 (16.21%)

anomaly in EA (Luo *et al.*, 2017c). The correlation map shows that the SST pattern is likely related to EA cold anomaly: positive correlations to the west of 50°W in lower latitudes and to the east of 30°W in higher latitudes, while negative correlations are apparent near Greenland (Figure 1e). To obtain a deeper understanding of the cold anomaly in EA, it is of interest to study the

relationships between the EA cold anomaly and typical SST patterns over the North Atlantic, especially making

OF1 (18.17%)

(a)

out the roles of atmospheric circulations and BKS sea ice loss.

# 3.1 | EOF analysis of North Atlantic SST anomalies

The first four EOF modes of SST are shown in Figure 2a. EOF1 represents widespread warming over the North

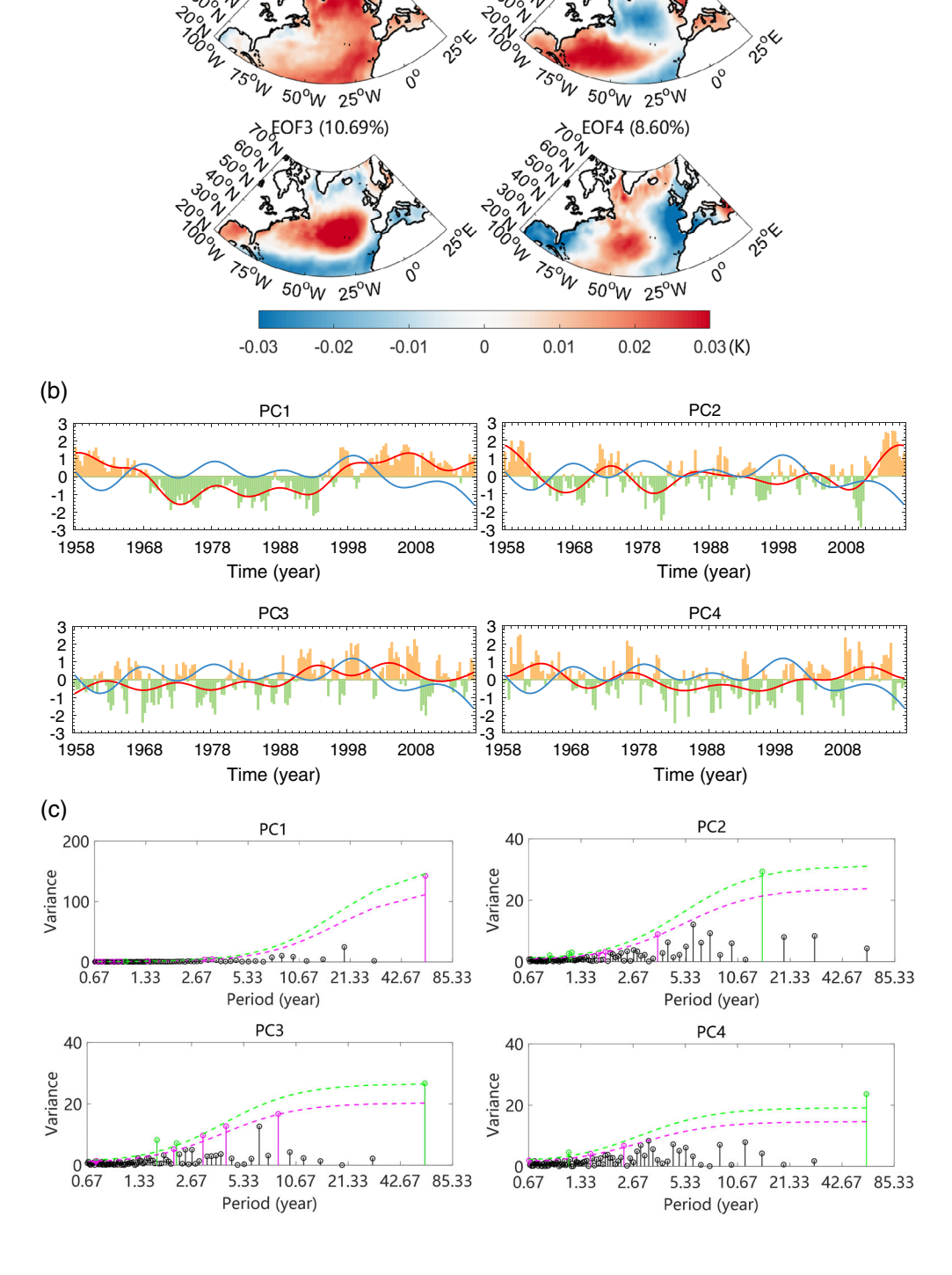


FIGURE 2 (a) The four leading EOFs (9 EOF1, EOF2, EOF3 and EOF4) of the detrended normalized SST anomalies in winter (December, January and February) during the time period 1958-2016. (b) Time series of the normalized principal components (PC1, PC2, PC3 and PC4) of EOF1, EOF2, EOF3 and EOF4 (bars) during 1958-2016. The red and blue solid lines represent the time variations of PCs and BKS SIC anomalies for time periods ≥10 years. (c) Power spectrums of the SST indices for normalized PC1, PC2, PC3 and PC4 calculated by fast Fourier transform (FFT). Green (violet) bars denote the periods that are significant at the 95% (90%) confidence level and the green (violet) dashed line denote the 95% (90%) confidence level line calculated by the lag-1 autocorrelation [Colour figure can be viewed at wileyonlinelibrary.com]

Atlantic basin. EOF2 resembles a north-south tripolar SST pattern, whereas EOF3 is a north-south tripolar mode located more northward of EOF2. EOF4 shows a west-east SST dipole pattern, which could be related to a midlatitude wave train that contributes to EA cold anomalies as proposed by Zhong et al. (2018). To understand how the amplitude of each EOF varies with time, Figure 2b shows the four normalized PC time series of the four leading EOF modes. Through checking the lead-lag relationships between the four PCs, we find no correlation coefficient being significant even at the 0.1 significance level. Furthermore, the correlation coefficient between PC1 and the AMO index is 0.93 (p < .01), which suggests that this mode very likely reflects the variability of the AMO pattern. It is clear that the PC2 stays in its positive phase after 2012, during which the Atlantic "cold blob" persists (Rahmstorf et al., 2015; Allan and Allan, 2019). PC3 is the only PC yielding a significant negative correlation (-0.32, p < .1) with the BKS SIC index. The cold anomaly in EA is more likely to be related to the EOF4 mode, because only PC4 shows a significant negative correlation (-0.32, p < 0.05) with the SAT in EA. Nevertheless, as we will indicate below, these SST modes may likely affect the EA cold anomaly once they are combined with the BKS SIC decline.

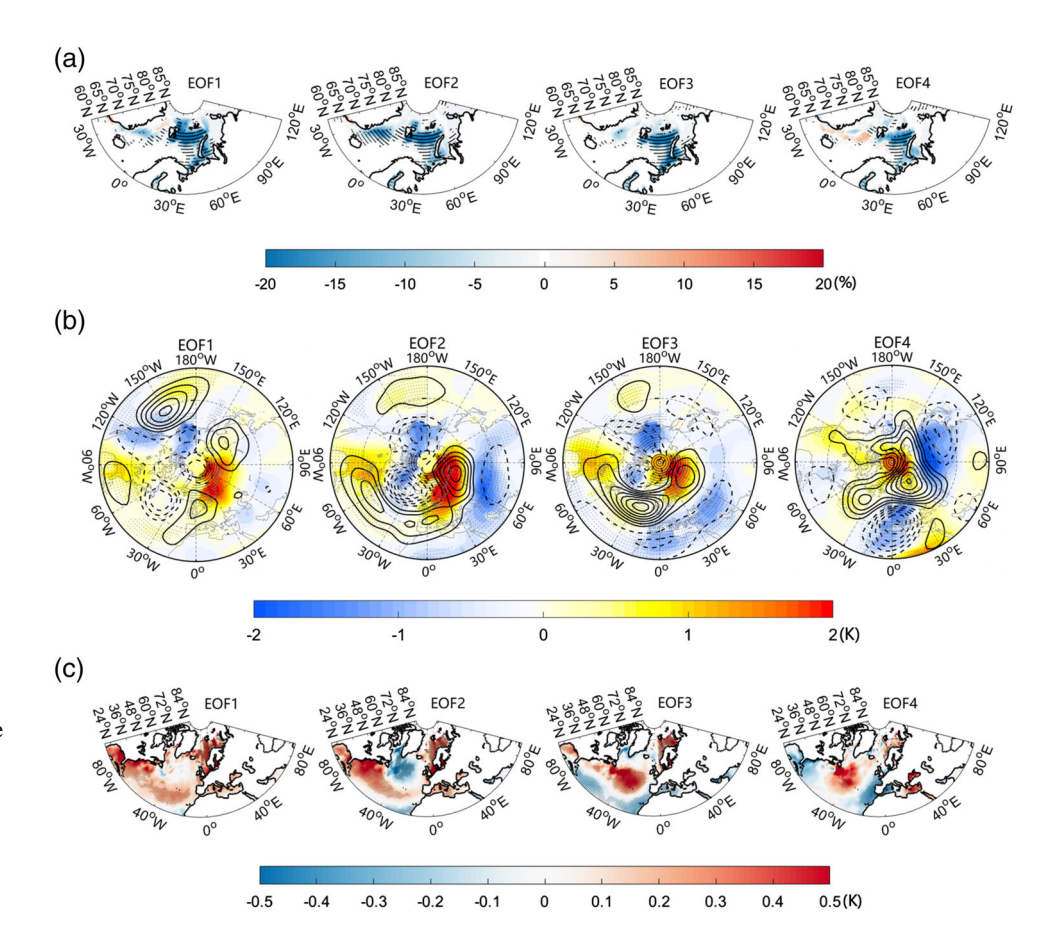
Fourier spectral analysis of the four PCs (Figure 2c) shows that PC1 only has significant multidecadal variations of about 60 years (p < .1), whereas PC2 exhibits

distinct interannual and decadal variations of about 3.69 (p < .1) and 14.75 (p < .05) years, respectively. Both PC3 and PC4 show significant interannual and multidecadal variations (p < .05). These results reflect the variabilities in the four leading SST modes on multidecadal, decadal and interannual timescales. This leads us to decompose the PCs into interannual timescales with time periods <10 years and decadal timescales with time periods ≥10 years to determine the relationships among the cold anomaly in EA, the North Atlantic SST modes and the BKS SIC on different timescales. In addition, BKS sea ice index shows opposite variations with the four PCs on decadal time scales although their correlation coefficients are not significant considering the effective degrees of freedom (Figure 2b). On interannual timescales, the BKS sea ice only has a significant negative relationship with PC3. It may be due to the warming region over the Gulf Stream Extension (Figure 2a), which has been studied by Sato et al. (2014) and Simmonds and Govekar (2014).

# 3.2 | Variabilities on interannual timescales

We here define an EOF to be in its positive phase when its normalized PC value is  $\geq 0.5$  SD. We also define the value of the normalized monthly mean SIC anomaly

FIGURE 3 Composite monthly mean (a) SIC anomalies (colour shading), (b) 500 hPa geopotential height (Z500) anomalies (contours, interval = 10gpm) and SAT anomalies (colour shading) and (c) SST anomalies (colour shading) of EOF1 (15 months), EOF2 (21 months), EOF3 (24 months) and EOF4 (12 months) for the normalized principal component indices with values equal to +0.5 STD or larger overlapped with a strong decrease in sea ice in the BKS with values equal to -0.5 STD or less for time periods <10 years during 1958-2016. For the SIC anomalies, SAT anomalies and SST anomalies the dots represent the area above the 95% confidence level for a twosided Student's t test [Colour figure can be viewed at wileyonlinelibrary.com]



with  $\leq -0.5$  (> -0.5) SD as a strong (weak) SIC decline. We further refer to the positive EOF mode overlapped with strong (weak) decrease in sea ice as the EOF mode with strong (weak) decrease in sea ice. The composite results show that when there is a large sea ice decrease in the BKS (Figure 3a), the UBs related to teleconnection patterns are anchored in the BKS for EOF2, EOF3 and EOF4 (Figure 3b). Correspondingly, intense cold anomalies appear in EA for the EOF2 mode and most of Asia for the EOF4 mode, and the EOF3 mode shows a significant cold

anomaly in the lower latitudes of west Asia.

Corresponding to different cold anomaly patterns, the distributions of the SST anomalies are different. Compared with EOF1, EOF2 reflects an intensification of the SST tripolar structure in the mid- to high-latitude North Atlantic (Figure 3c). The associated circulation pattern is more distinct, with a positive North Atlantic Oscillation (NAO+) pattern and an UB, and it is related to cold anomalies in EA and west Asia. In the case of EOF3, the positive SST anomalies are displaced toward higher latitudes and the northern negative SST anomalies become weaker (Figure 3c). The NAO pattern over the North Atlantic is also situated more northward and has a more northwest-southeast orientation relative to the NAO+ pattern of EOF2. Continental cold anomaly weakens and shifts

towards west Asia (Figure 3b). For the SST pattern of EOF4 the SST anomalies show a west–east dipole mode, with positive (negative) SST anomalies in the west (east) (Figure 3c). Along with EOF4, a midlatitude wave train, resembling that shown by Zhong *et al.* (2018), is distinct over the North Atlantic, and continental cold anomaly is significant over EA and western Europe (Figure 3b). Although the positive SST anomaly (Figure 3c) or decrease in SIC is intense in the BKS (Figure 3a), the cold anomaly region is dependent on the shape of North Atlantic warming outside the Arctic region (Figure 3b). This at least suggests that we should consider the regional characters of North Atlantic warming to understand the regional change in the cold anomaly over Eurasia even when the decrease in SIC is strong in the BKS.

When the BKS SIC either decreases weakly or increases (Figure 4a), the atmospheric teleconnection patterns in response to the SST anomalies in the North Atlantic show clear zonal wave train structures from the North Atlantic to Eurasia (Figure 4b). Although blocking anticyclones can appear over Eurasia for each of the EOFs, they are not anchored in the Ural region and are relatively weak (Figure 4b). In this case, no intense cold anomaly can be seen in EA for these SST modes. Compared with Figure 3c, the absence of cold anomaly over EA is not only

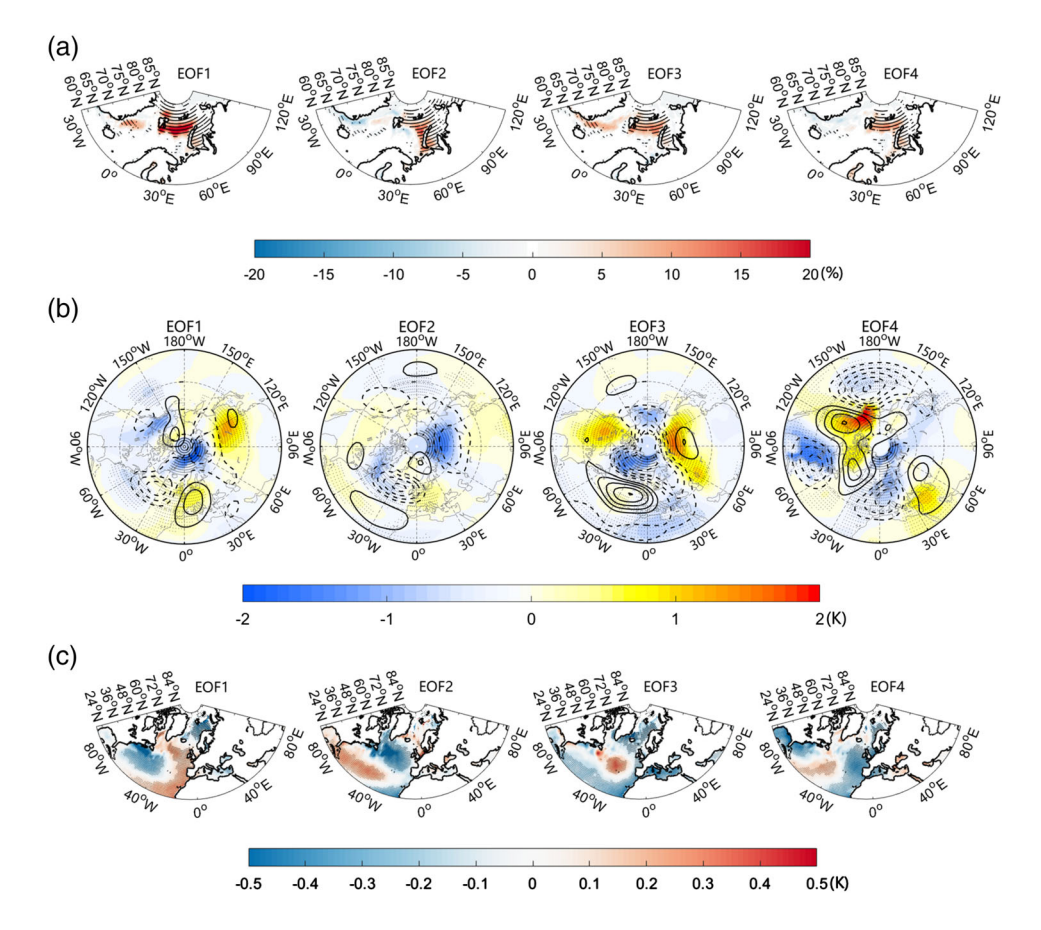


FIGURE 4 Composite monthly mean (a) SIC anomalies (colour shading), (b) Z500 anomalies (contours, interval = 10gpm) and SAT anomalies (colour shading) and (c) SST anomalies (colour shading) of EOF1 (40 months), EOF2 (35 months), EOF3 (33 months) and EOF4 (41 months) for the normalized principal component indices with values equal to +0.5 STD or larger overlapped with a strong decrease in sea ice in the BKS with values larger than −0.5 STD for time periods <10 years during 1958–2016. For the SIC anomalies, SAT anomalies and SST anomalies the dots represent the area above the 95% confidence level for a twosided Student's t test [Colour figure can be viewed at wileyonlinelibrary.com]

associated with the weak decrease or increase in BKS SIC (Figure 4a), but also to the weak warming in the mid- to high-latitude North Atlantic (Figure 4c).

## 3.3 | Variabilities on decadal timescales

We now investigate the roles of the SST and SIC anomalies with timescales ≥10 years (Figure 5). The positive SST anomalies (Figure 5c) in the North Atlantic are more widespread on decadal timescales, when the SIC in the BKS exhibits a large decrease (Figure 5a). However, atmospheric circulation patterns are not as clear and organized as those on interannual timescales. The atmospheric response shows a UB pattern only for EOF1 and EOF4, although the UB pattern is located more to the east for EOF1 (Figure 5b). In this case, significant decadal cold anomalies can be seen over EA for EOF1 and EOF4 (Figure 5b), which is weaker than the interannual cold anomalies (Figure 3b). Notably, the positive SST anomalies (Figure 5c) in the North Atlantic and the BKS are stronger and more widespread than those on interannual timescales (Figure 3c), and the anticyclone over the BKS is weaker and even absent for EOF2 and EOF3 modes (Figure 5b). This suggests that the decadal decrease in BKS SIC is more of an Arctic oceanic process and is

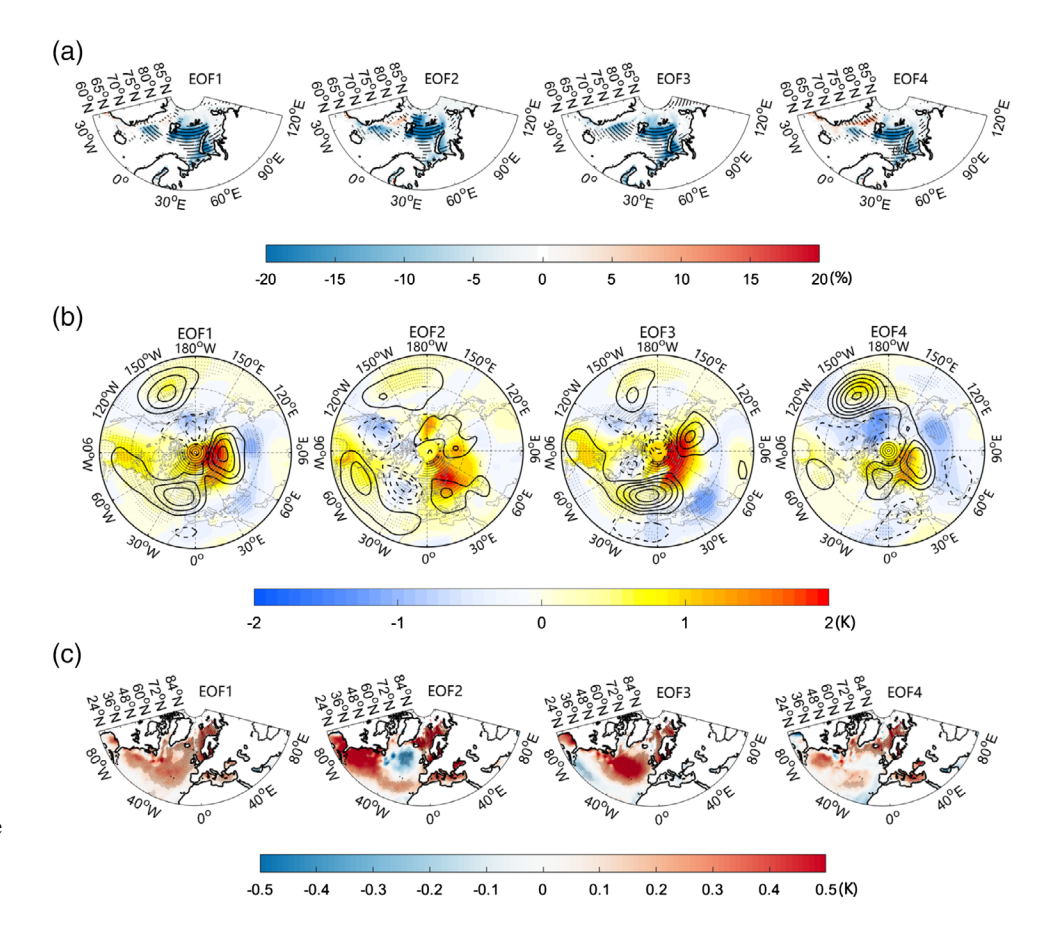
probably related to the poleward transport of North Atlantic warm water (Alexeev *et al.*, 2013) or warming in the BKS. This indirectly suggests that, on interannual timescales, the associated atmospheric circulation patterns (Figure 3b) may play a more important part in the change in the BKS SIC via the change in downward infrared radiation (Woods and Caballero, 2016; Lee *et al.*, 2017; Luo *et al.*, 2017a; Zhong *et al.*, 2018).

Composite results without filtering for the four PCs were also analysed (Figure 6). Combined with the above analysis, the cold anomaly over EA is related to EOF1 with decadal variations, EOF2 with interannual variations and EOF4 with both interannual and decadal variations. However, the EA cold anomaly with EOF2 seems to be offset by its interannual variabilities and decadal variabilities (Figure 6a). No intense cold anomaly can be seen in EA for cases without a large decrease in the BKS SIC and the atmospheric responses also show typical wave train structures (Figure 6b).

# 3.4 | Anchoring of the Ural blocking anticyclone

We mentioned earlier in this study that the large decrease in the BKS SIC could affect the cold anomaly over EA

FIGURE 5 Composite monthly mean (a) SIC anomalies (colour shading), (b) Z500 anomalies (contours, interval = 10gpm) and SAT anomalies (colour shading) and (c) SST anomalies (colour shading) of EOF1 (33 months), EOF2 (16 months), EOF3 (20 months) and EOF4 (21 months) for the normalized principal component indices with values equal to +0.5 STD or larger overlapped with a strong decrease in sea ice in the BKS with values equal to -0.5 STD or less for time periods ≥10 years during 1958-2016. For the SIC anomalies, SAT anomalies and SST anomalies the dots represent the area above the 95% confidence level for a twosided Student's t test [Colour figure can be viewed at wileyonlinelibrary.com]





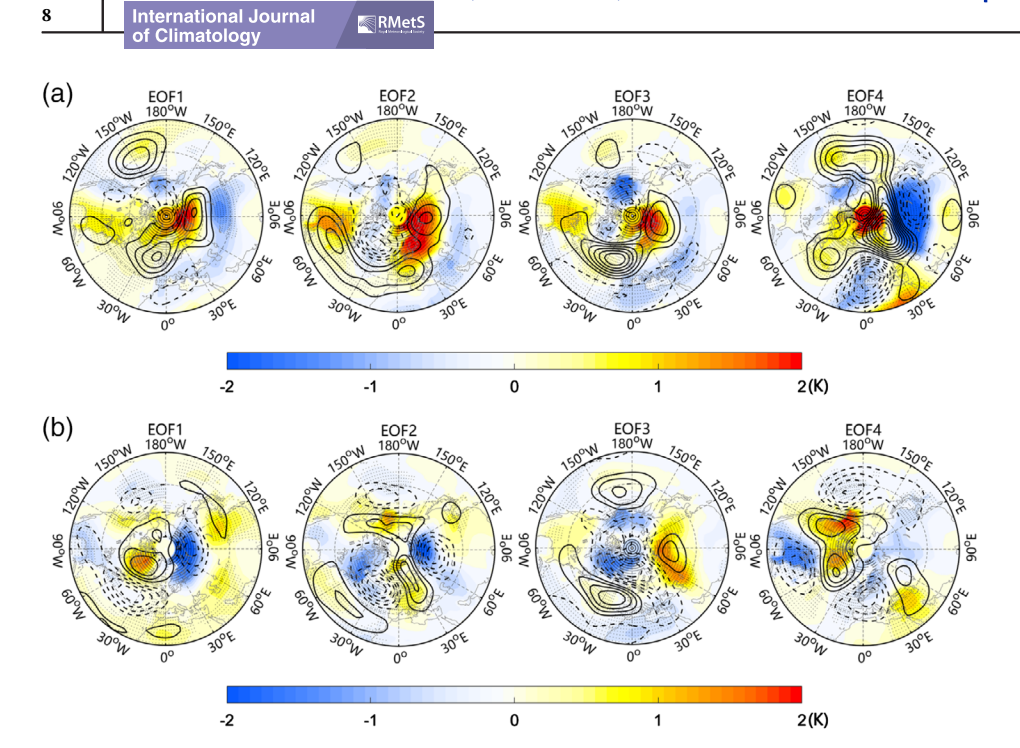


FIGURE 6 Composite monthly mean Z500 anomalies (contours. interval = 10 gpm) and SAT anomalies (colour shading) of EOF1, EOF2, EOF3 and EOF4 for normalized principal component indices with values equal to +0.5 STD or larger overlapped with (a) strong decrease in the BKS SIC with values equal to -0.5 STD or less and (b) weak decrease in the BKS SIC with values larger than -0.5 STD during the time period 1958-2016. For the SAT anomalies, the dots represent the area above the 95% confidence level for a two-sided Student's t test [Colour figure can be viewed at wileyonlinelibrary.com]

through UB on both interannual and decadal timescales, although it is coupled with the SST in the BKS and the atmospheric circulation. Here, we further illustrate the role of the BKS SIC loss in anchoring the UB from the daily variation of UB (Figure 7). To quantify the persistence of the UBs, we showed the time-longitude evolution of the composite Z500 anomalies averaged over 50-70°N for the UBs and calculated their travelling speeds using the slopes of arrows in Figure 7. It is noted that the speeds of UBs with strong decrease in the BKS SIC are all  $0^{\circ}$ /day ( $0^{\circ}$ /day,  $4.23^{\circ}$ /day,  $0.24^{\circ}$ /day,  $0^{\circ}$ /day), while UBs travel at 13.33°/day, 0.31°/day, 10.67°/day, 10.63°/day (13.89°/day, 1.67°/day, 5.67°/day, 10.67°/day) with weak decrease in the BKS SIC on interannual timescales (decadal timescales) for the four EOFs. It is evident that the UB is more quasi-stationary for conditions with a strong decrease in the BKS SIC (Figure 7a,c) than those without a large decrease in SIC (Figure 7b,d) both on interannual time scales and decadal timescales. Although the UB in EOF2 does not show clear movement with a weak decrease or increase in SIC, it has a much weaker intensity and a shorter lifetime (Figure 7b,d). In addition, previous studies provided evidence to support the proposition that the large decrease in BKS SIC prior to the onset of blocking can make the UB more stationary and persistent through the weakening of zonal winds in Eurasia and the strengthening of zonal winds in the midhigh latitude North Atlantic (Luo et al., 2016; Gong and Luo, 2017; Yao et al., 2017; Luo et al., 2017b; Chen et al., 2018b). As a result, although the UB arises from a teleconnection pattern initiated from the North Atlantic,

the large decrease in the BKS SIC (related to warming in the BKS) can anchor the UB and increase its persistence, which can intensify cold anomaly over EA. It should be mentioned that in this paper we did not discuss the effect of UB in November on winter Eurasian cold anomaly probably through the winter polar vortex change related to autumn vertically propagating planetary waves (Peings, 2019). This issue needs to be further studied.

# 4 | DISCUSSION AND CONCLUSIONS

Correlation analysis, EOF analysis and composite analysis are used to examine the role of BKS SIC and North Atlantic SST in winter cold anomaly over EA. We obtained four SST modes through an EOF analysis, these taking the forms of a basin-scale warming mode, two north-south tripolar modes (with different locations) and an east-west dipole mode. Through performing a Fourier analysis on the four PCs of the EOF modes, we find that both interannual and decadal timescales should be considered when investigating how SSTs in the North Atlantic affect the cold anomaly over EA. We comment that the variances explained by EOF1 and EOF2 are similar (Figure 2a) and this bears on their separability. A number of studies (e.g., Roundy, 2015) have demonstrated that EOF modes of nearly identical variances can be profitably combined by taking linear combinations to describe evolving physical patterns. In our case, the relationship between SST modes and EA temperature could be

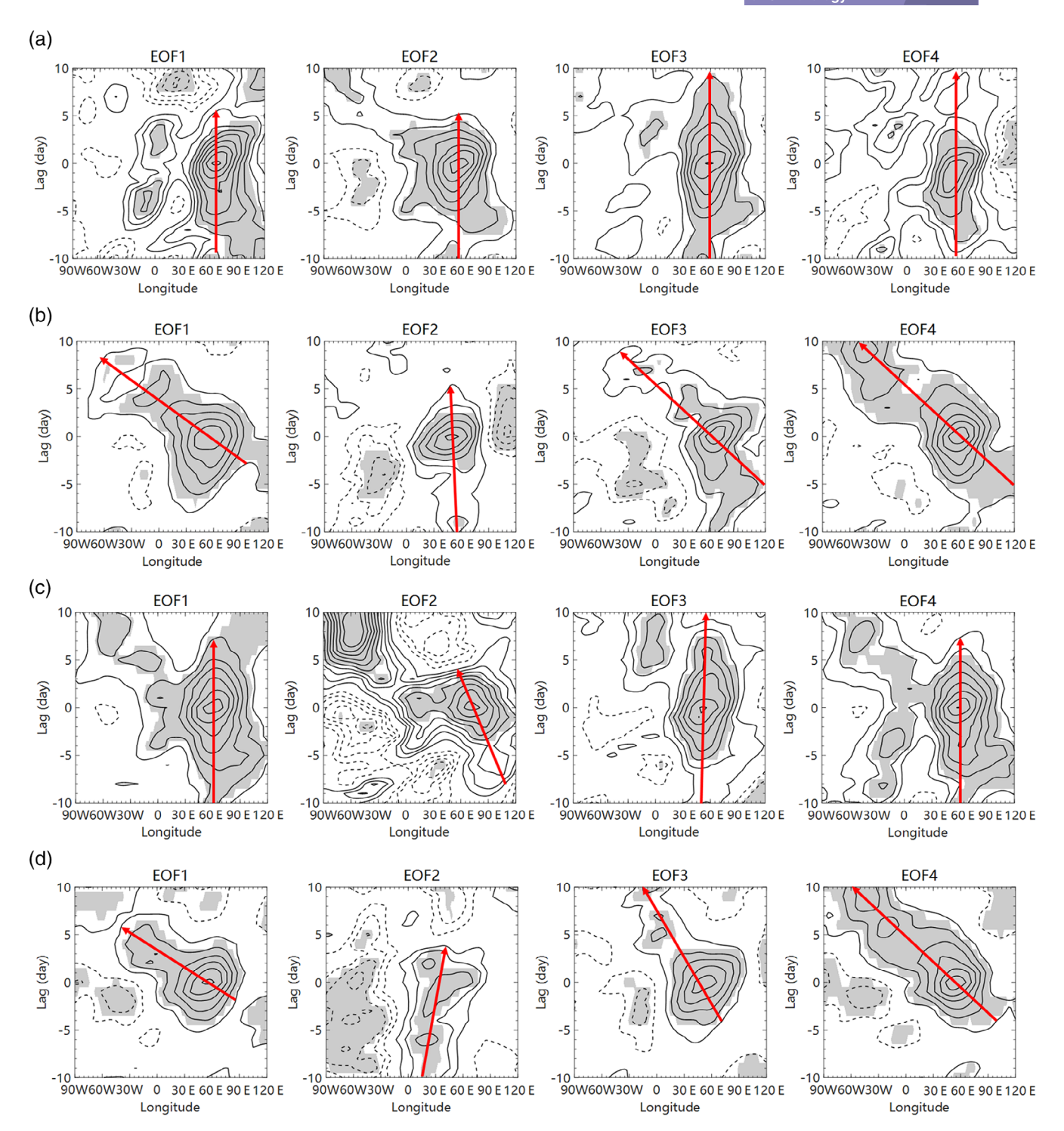


FIGURE 7 Time-longitude evolution of composite daily Z500 anomalies of Ural blocking events averaged over  $50-80^{\circ}$ N of EOF1, EOF2, EOF3 and EOF4 for PCs with values equal to +0.5 STD or larger for (a), (b) time periods <10 years and (c), (d) time periods  $\ge10$  years with (a), (c) less and (b), (d) more SIC anomalies. Grey shading denotes areas with Z500 anomalies significant at the 95% confidence level based on a Monte-Carlo test with 10,000 simulations [Colour figure can be viewed at wileyonlinelibrary.com]

enhanced (i.e., achieve a higher correlation) by using a linear addition of our first two modes. However, we have decided not to take this extra step here.

On interannual timescales, the more southward north-south tripolar SST pattern and the east-west

dipole SST pattern are related to the cold anomaly over EA when there is strong SIC decline in the BKS. However, with weakly decreased or increased SIC in the BKC, there is no intense cooling in EA and the atmospheric circulation shows a wave train structure. On decadal

LI ET AL.

timescales, the basin-scale warming and the east—west dipole SST pattern are linked to the cold anomaly over EA which is weaker than that on interannual timescales. In addition, on both interannual and decadal timescales, the UBs are located over the BKS region for the EA cold anomaly cases. Although the large decrease in BKS SIC can anchor the position of UB, the shape of North Atlantic warming could affect the position of cold anomaly over EA by altering the pathway of the teleconnection pattern from North Atlantic to Eurasia. This is different from previous studies (Sato *et al.*, 2014; Jung *et al.*, 2017; Liu *et al.*, 2018), since these studies only focus on the role of teleconnections originating from the Gulf Stream Extension in the warming over BKS and cold anomaly over Eurasia.

Moreover, UB, which is related to EA cold anomaly, seems to result from the teleconnection pattern excited by warming of the SST in the North Atlantic. Whether UB has an important effect on the cold anomaly in EA depends significantly on whether there is a large negative SIC anomaly over the BKS. When the decrease in the BKS SIC is large, strong cold anomalies can take place over EA as a result of both less movement and increased persistence of UB. However, when there is only a small decrease in the BKS SIC, then UB moves rapidly and has little effect on the cold anomaly over EA.

Finally, it should be pointed out that this study only focuses on the impacts of sea ice loss in the BKS on EA cold anomaly. However, as shown in Figure 1d, both the sea ice loss in the BKS and sea ice increase in the Greenland Sea have significant relationships with EA cold anomaly. This indicates that the SIC change in the Greenland Sea may also play a role in linking the atmospheric circulations to EA cold anomaly (Chen and Luo, 2017) and relevant research will be carried out in the future. In addition, since effective sample size should be considered when studying the relationships among BKS sea ice change, Atlantic SST modes and winter cold anomaly in EA, large-ensemble simulated data as by the Polar Amplification Intercomparison Project (PAMIP) are expected to apply to further researches.

## **ACKNOWLEDGEMENTS**

We acknowledge support from the Chinese Academy of Science Strategic Priority Research Program (Grant XDA 19070403) and the National Key Research and Development Program of China (2016YFA0601802). Simmonds was supported by Australian Research Council Grant DP16010997. Dai acknowledges the funding support from the U.S. National Science Foundation (Grant No. OISE-1743738) and the U.S. National Oceanic and Atmospheric Administration (Award NA18OAR4310425).

#### ORCID

*Linhao Zhong* https://orcid.org/0000-0003-2833-1808 *Yao Yao* https://orcid.org/0000-0002-6425-7855

#### REFERENCES

- Alexeev, V.A., Ivanov, V.V., Kwok, R. and Smedsrud, L.H. (2013) North Atlantic warming and declining volume of Arctic Sea ice. *The Cryosphere Discuss.*, 7, 245–265. https://doi.org/10. 5194/tcd-7-245-2013.
- Allan, D. and Allan, R.P. (2019) Seasonal changes in the North Atlantic cold anomaly: the influence of cold surface waters from coastal Greenland and warming trends associated with variations in subarctic sea ice cover. *Journal of Geophysical Research*, 124, 9040–9052. https://doi.org/10.1029/2019JC015379.
- Chen, L.L., Francis, J. and Hanna, E. (2018a) The "warm-Arctic/cold-continents" pattern during 1901–2010. *International Journal of Climatology*, 38(14), 524–5254. https://doi.org/10.1002/joc.5725.
- Chen, X. and Luo, D. (2017) Arctic Sea ice decline and continental cold anomalies: upstream and downstream effects of Greenland blocking. *Geophysical Research Letters*, 44, 3411–3419. https://doi.org/10.1002/2016GL072387.
- Chen, X., Luo, D., Feldstein, S. and Lee, S. (2018b) Impact of winter Ural blocking on Arctic Sea ice: short-time variability. *Journal of Climate*, 31(6), 2267–2282. https://doi.org/10.1175/Jcli-D-17-0194.1.
- Cohen, J., Pfeiffer, K. and Francis, J.A. (2018) Warm Arctic episodes linked with increased frequency of extreme winter weather in the United States. *Nature Communications*, 9, 869. https://doi.org/10.1038/s41467-018-02992-9.
- Cohen, J., Screen, J.A., Furtado, J.C., Barlow, M., Whittleston, D., Coumou, D., Francis, J., Dethloff, K., Entekhabi, D., Overland, J. and Jones, J. (2014) Recent Arctic amplification and extreme mid-latitude weather. *Nature Geoscience*, 7(9), 627–637. https://doi.org/10.1038/ngeo2234.
- Dai, A., Fyfe, J.C., Xie, S.-P. and Dai, X. (2015) Decadal modulation of global surface temperature by internal climate variability. *Nature Climate Change*, 5(6), 555–559. https://doi.org/10.1038/ nclimate2605.
- Dai, A. and Song, M. (2020) Little influence of Arctic amplification on midlatitude climate. *Nature Climate Change*, 10, 231–237. https://doi.org/10.1038/s41558-020-0694-3.
- Deser, C. and Blackmon, M.L. (1993) Surface climate variations over the North Atlantic Ocean during winter: 1900-1989. *Journal of Climate*, 6(9), 1743–1753. https://doi.org/10.1175/1520-0442(1993)006<1743:SCVOTN>2.0.CO;2.
- Gong, T. and Luo, D. (2017) Ural blocking as an amplifier of the Arctic Sea ice decline in winter. *Journal of Climate*, 30(7), 2639–2654. https://doi.org/10.1175/JCLI-D-16-0548.1.
- Gulev, S.K., Latif, M., Keenlyside, N., Park, W. and Koltermann, K. P. (2013) North Atlantic Ocean control on surface heat flux on multidecadal timescales. *Nature*, 499(7459), 464–467. https://doi.org/10.1038/nature12268.
- Hansen, J., Ruedy, R., Sato, M. and Lo, K. (2010) Global surface temperature change. *Reviews of Geophysics*, 48, 29. https://doi. org/10.1029/2010rg000345.
- Jung, O., Sung, M.-K., Sato, K., Lim, Y.-K., Kim, S.-J., Baek, E.-H., Jeong, J.-H. and Kim, B.-M. (2017) How does the SST variability

LI ET AL.

- over the western North Atlantic Ocean control Arctic warming over the Barents-Kara seas? *Environmental Research Letters*, 12 (3), 034021. https://doi.org/10.1088/1748-9326/aa5f3b.
- Kalnay, E., Kanamitsu, M., Kistler, R., Collins, W., Deaven, D., Gandin, L., Iredell, M., Saha, S., White, G., Woollen, J., Zhu, Y., Leetmaa, A., Reynolds, R., Chelliah, M., Ebisuzaki, W., Higgins, W., Janowiak, J., Mo, K.C., Ropelewski, C., Wang, J., Jenne, R. and Joseph, D. (1996) The NCEP/NCAR 40-year reanalysis project. *Bulletin of the American Meteorological Society*, 77(3), 437–471. https://doi.org/10.1175/1520-0477(1996) 077<0437:TNYRP>2.0.CO;2.
- Kug, J.-S., Jeong, J.-H., Jang, Y.-S., Kim, B.-M., Folland, C.K., Min, S.-K. and Son, S.-W. (2015) Two distinct influences of Arctic warming on cold winters over North America and East Asia. *Nature Geoscience*, 8(10), 759–762. https://doi.org/10.1038/ ngeo2517.
- Lee, S., Gong, T.T., Feldstein, S.B., Screen, J.A. and Simmonds, I. (2017) Revisiting the cause of the 1989–2009 Arctic surface warming using the surface energy budget: downward infrared radiation dominates the surface fluxes. *Geophysical Research Letters*, 44(20), 10654–10661. https://doi.org/10.1002/2017GL075375.
- Li, S. (2004) Impact of Northwest Atlantic SST anomalies on the circulation over the Ural Mountains during early winter. *Journal of the Meteorological Society of Japan*, 82(4), 971–988. https://doi.org/10.2151/jmsj.2004.971.
- Liu, X., Xu, Z., Peng, D. and Wu, G. (2018) Influences of the North Atlantic oscillation on extreme temperature during the cold period in China. *International Journal of Climatology*, 39(1), 43–49. https://doi.org/10.1002/joc.5779.
- Luo, B., Luo, D., Wu, L., Zhong, L. and Simmonds, I. (2017c) Atmospheric circulation patterns which promote winter Arctic Sea ice decline. *Environmental Research Letters*, 12(5), 054017. https://doi.org/10.1088/1748-9326/aa69d0.
- Luo, D., Chen, Y., Dai, A., Mu, M., Zhang, R. and Simmonds, I. (2017b) Winter Eurasian cooling linked with the Atlantic multidecadal oscillation. *Environmental Research Letters*, 12(12), 125002. https://doi.org/10.1088/1748-9326/aa8de8.
- Luo, D., Xiao, Y., Yao, Y., Dai, A., Simmonds, I. and Franzke, C.L. E. (2016) Impact of Ural blocking on winter warm Arctic-cold Eurasian anomalies. Part I: blocking-induced amplification. *Journal of Climate*, 29(11), 3925–3947. https://doi.org/10.1175/jcli-d-15-0611.1.
- Luo, D., Yao, Y., Dai, A., Simmonds, I. and Zhong, L. (2017a) Increased quasi-stationarity and persistence of Ural blocking and Eurasian extreme cold events in response to Arctic warming. Part II: a theoretical explanation. *Journal of Climate*, 30(10), 3569–3587. https://doi.org/10.1175/JCLI-D-16-0262.1.
- McCusker, K.E., Fyfe, J.C. and Sigmond, M. (2016) Twenty-five winters of unexpected Eurasian cooling unlikely due to Arctic Sea ice loss. *Nature Geoscience*, 9(11), 838–843. https://doi.org/ 10.1038/NGEO2820.
- Mori, M., Watanabe, M., Shiogama, H., Inoue, J. and Kimoto, M. (2014) Robust Arctic Sea-ice influence on the frequent Eurasian cold winters in past decades. *Nature Geoscience*, 7(12), 869–873. https://doi.org/10.1038/ngeo2277.
- Outten, S. and Esau, I. (2012) A link between Arctic Sea ice and recent cooling trends over Eurasia. *Climatic Change*, 110, 1069–1075. https://doi.org/10.1007/s10584-011-0334-z.

- Peings, Y. (2019) Ural blocking as a driver of early winter stratospheric warming. *Geophysical Research Letters*, 46(10), 5460–5468. https://doi.org/10.1029/2019GL082097.
- Petoukhov, V. and Semenov, V. (2010) A link between reduced Barents-Kara Sea ice and cold winter extremes over northern continents. *Journal of Geophysical Research-Atmospheres*, 115, D21111. https://doi.org/10.1029/2009jd013568.
- Rahmstorf, S., Box, J.E., Feulner, G., ME, M.M., Robinson, A., Rutherford, S. and Schaffernicht, E.J. (2015) Exceptional twentieth-century slowdown in Atlantic Ocean overturning circulation. *Nature Climate Change*, 5, 475–480. https://doi.org/ 10.1038/nclimate2554.
- Raspopov, O.M., Kuz'Min, I.A. and Kharin, E.P. (2007) The 50th anniversary of international geophysical year (1957-1958): from the first international polar year (1882-1883) to the international Heliophysical year (2007-2008) and international polar year (2007-2009). *Geomagnetism and Aeronomy*, 47(1), 1–7. https://doi.org/10.1134/S001679320701001x.
- Rayner, N.A., Parker, D.E., Horton, E.B., Folland, C.K., Alexander, L. V., Rowell, D.P., Kent, E.C. and Kaplan, A. (2003) Global analyses of sea surface temperature, sea ice, and night marine air temperature since the late nineteenth century. *Journal of Geophysical Research-Atmospheres*, 108(D14), 4407. https://doi.org/10.1029/2002JD002670.
- Roundy, P.E. (2015) On the interpretation of EOF analysis of ENSO, atmospheric Kelvin waves, and the MJO. *Journal of Climate*, 28, 1148–1165. https://doi.org/10.1175/JCLI-D-14-00398.1.
- Sato, K., Inoue, J. and Watanabe, M. (2014) Influence of the Gulf stream on the Barents Sea ice retreat and Eurasian coldness during early winter. *Environmental Research Letters*, 9(8), 084009. https://doi.org/10.1088/1748-9326/9/8/084009.
- Screen, J.A., Deser, C., Simmonds, I. and Tomas, R. (2014) Atmospheric impacts of Arctic Sea-ice loss, 1979-2009: separating forced change from atmospheric internal variability. *Climate Dynamics*, 43, 333–344. https://doi.org/10.1007/s00382-013-1830-9.
- Screen, J.A. and Simmonds, I. (2010) The central role of diminishing sea ice in recent Arctic temperature amplification. *Nature*, 464 (7293), 1334–1337. https://doi.org/10.1038/nature09051.
- Screen, J.A., Simmonds, I., Deser, C. and Tomas, R. (2013) The atmospheric response to three decades of observed Arctic Sea ice loss. *Journal of Climate*, 26, 1230–1248. https://doi.org/10. 1175/JCLI-D-12-00063.1.
- Simmonds, I. (2015) Comparing and contrasting the behaviour of Arctic and Antarctic Sea ice over the 35-year period 1979-2013. Annals of Glaciology, 56(69), 18–28. https://doi.org/10.3189/2015AoG69A909.
- Simmonds, I. and Govekar, P.D. (2014) What are the physical links between Arctic Sea ice loss and Eurasian winter climate? *Environmental Research Letters*, 9(10), 101003. https://doi.org/10.1088/1748-9326/9/10/101003.
- Steinman, B.A., Mann, M.E. and Miller, S.K. (2015) Atlantic and Pacific multidecadal oscillations and northern hemisphere temperatures. *Science*, 347(6225), 988–991. https://doi.org/10.1126/science.1257856.
- Tibaldi, S. and Molteni, F. (1990) On the operational predictability of blocking. *Tellus*, 42A, 343–365. https://doi.org/10.1034/j. 1600-0870.1990.t01-2-00003.x.

International Journal of Climatology

**₹** RMetS

LI ET AL.

- Walsh, J.E. (2014) Intensified warming of the Arctic: causes and impacts on middle latitudes. *Global and Planetary Change*, 117, 52–63. https://doi.org/10.1016/j.gloplacha.2014.03.003.
- Woods, C. and Caballero, R. (2016) The role of moist intrusions in winter Arctic warming and sea ice decline. *Journal of Climate*, 29(12), 4473–4485. https://doi.org/10.1175/jcli-d-15-0773.1.
- Yao, Y., Luo, D., Dai, A. and Simmonds, I. (2017) Increased quasistationarity and persistence of Ural blocking and Eurasian extreme cold events in response to Arctic warming. Part I: insight from observational analyses. *Journal of Climate*, 30(10), 3549–3568. https://doi.org/10.1175/JCLI-D-16-0261.1.
- Zhong, L., Hua, L. and Luo, D. (2018) Local and external moisture sources for the Arctic warming over the Barents-Kara seas.

*Journal of Climate*, 31(5), 1963–1982. https://doi.org/10.1175/ JCLI-D-17-0203.1.

How to cite this article: Li M, Luo D, Simmonds I, Dai A, Zhong L, Yao Y. Anchoring of atmospheric teleconnection patterns by Arctic Sea ice loss and its link to winter cold anomalies in East Asia. *Int J Climatol*. 2020;1–12. <a href="https://doi.org/10.1002/joc.6637">https://doi.org/10.1002/joc.6637</a>